Quenching of Li* by N_2: A Dual Theoretical MO–CI and VB Investigation of the Role of Ionic and Covalent Surfaces

Alain Sevin,*,‡ Patrick Chaquin,‡ Louis Hamon,‡ and Philippe C. Hiberty§

Contribution from the Laboratoire de Chimie Organique Théorique, Bât. F, 4 Place Jussieu, 75252 Paris Cédex 05, France, and Laboratoire de Chimie Théorique,† Bât. 490, Centre d'Orsay, 91405 Orsay Cédex, France. *Received December 18, 1987*

Abstract: The potential energy surfaces for the quenching of the low-lying states (≤5 eV) have been calculated with independent MO–CI and VB methods. The MO–CI calculations show that the quenching is more effective in the C_{2v} geometry than in the linear one. The relaxation of N_2, up to the equilibrium distance of N_2^-, is essential at a short distance of approach, since it allows for a contact between the GS and the lowest excited surfaces, in both geometries. The VB analysis, in a model linear study, clearly points out the leading role of the quasi-diabatic charge-transfer surface ($Li^+\cdots N_2^-$), which crosses the covalent ($Li^*\cdots N_2$) surfaces, thus adiabatically yielding a lowest energy exciplex bearing an ionic:covalent ratio of 44:56.

The quenching of alkali and alkali-earth atoms by small molecules has been widely studied, by both experimentalists and theoreticians.[1-6] Pioneer works[7-9] have pointed out the fact that the link channel between the essentially repulsive covalent surfaces of approach of the (M···AB) ground state (GS) and the lowest excited state (M*···AB) might be provided by the ionic surface ($M^+\cdots AB^-$), in a diabatic scheme. Indeed, the resulting diabatic crossings are masked in an adiabatic calculation where only exciplex formation can be put to the fore. However, although Nikitin's ionic model is adequate either for molecules having a strong electron affinity, such as dihalogens,[10,11] or for very polar moieties such as HX,[12,13] it is no longer effective with molecules of very low electron affinity such as H_2 or hydrocarbons. In the latter case, it has been theoretically established[14-16] that a small stretching of H_2 allows for the formation of triangular exciplexes, bearing a dominant covalent character.

In this perspective, N_2 is a challenging molecule since it might be thought that ionic exciplexes have some stability but π delocalization might also stabilize covalent species to some extent; hence, a complex mixture of both can be expected. It is therefore of primary importance to estimate the relative weights of ionic and covalent mechanisms in the actual process. We propose in what follows a model study of the quenching of an excited lithium atom by N_2. Previous calculations on the parent system (Na* + N_2) did not include electronic correlation,[8,9,17-21] and ab initio calculations are only available for the cationic $(Li + N_2)^+$ system.[22] Thus, our aim was dual: (i) to state the role of electronic correlation by calculating reliable SCF–CI potential surfaces for the low-energy states of the system in the range 0–6 eV; (ii) to point out the role of ionic and covalent surfaces in the quasi-diabatic scheme provided by a VB analysis of the process. A complementary use of both methods allows for a complete discussion of the quenching mechanism in terms of previously proposed methods.[1,5]

Theoretical Methods

MO–CI Calculations. Ab initio SCF–CI calculations were achieved with the Monstergauss series of programs[23] in the SCF step. Exploratory runs and geometry optimizations for the Li 2S and 2P states were done by first the 3-21G and then the 6-31G* basis sets.[24] A first CI was then carried out with a basis set that consists of 6-31G basis functions augmented by diffuse s + p functions on Li, of exponent 0.008. Through direct diagonalization of a limited reference set of configurations (≈100), the latter technique yields a good qualitative shape of the various energy surfaces (ESs). At last, a calculation of the correlation energy was carried out with the CIPSI Møller–Plesset algorithm,[25] with the 6-31G* basis set. The multireference set included about 100 Slater determinants, and the perturbation involved (1–3) × 10^6 terms. The RHF Davidson Hamiltonian[26] was used throughout. Selected calculated values (6-31G* + CIPSI), corresponding to the electronic configurations of Table I, are given in Table II.

Table I. Leading Terms in Electronic Configurations for the System Li + N_2 in Various Geometries[a]

confign	state of Li	$C_{\infty v}$	C_s	C_{2v}
...core...$(2s)^1$	2S	Σ^+	A′	A_1
...$(2p_x)^1$	2P	Π	A″	B_1
...$(2p_y)^1$			A′	B_2
...$(2p_z)^1$		Σ^+	A′	A_1
...$(\pi_x^*)^1$	CT	Π	A″	A_2
...$(\pi_y^*)^1$			A′	B_2

[a] The states of Li correspond to infinite separation. The symmetry labels in $C_{\infty v}$, C_s, and C_{2v} geometries, along with their correlations, are given with the axes defined in Figure 2.

Table II. Selection of Calculated Values by the 6-31G* + CIPSI Method[a]

$C_{\infty v}$	R	10.000	4.540	3.290	2.580	2.350	2.140	2.080
	r	1.078	1.078	1.078	1.169	1.169	1.169	1.169
	Σ^+	0.00[b]	0.02	−0.05	0.18	0.50	1.10	1.82
	Π	1.95[c]	1.92	1.51	1.07	1.03	1.10	1.16
	Σ^+	1.95	2.18	2.50	2.98			
	CT	8.03						
C_{2v}	R	2.000	1.900	1.800				
	r	1.169	1.169	1.169				
	A_1	0.38	0.48	0.55				
	B_2	0.51	0.48	0.46				
	B_1	1.66		2.40				
	A_2	1.72						

[a] The geometrical parameters are defined in Figure 2. [b] Absolute reference energy: −116.672 20 au. All data are in electronvolts. [c] Experimental values are the following: 2P, 1.85; 3S, 3.37; 3P, 3.83; 3D, 3.88; 4S, 4.34; 4P, 4.52. From: More, C. E. *Atomic Energy Levels*; National Bureau of Standards: Washington, DC, 1952; Vol. 1 and 2.

‡ Laboratoire de Chimie Organique Théorique.
§ Laboratoire de Chimie Théorique.
† Both laboratories form the UA No. 506 of the CNRS.

(1) Nikitin, E. E. *Theory of Atomic and Molecular Processes in Gases*; Oxford University: Oxford, 1974.
(2) Klabunde, K. J. *Chemistry of Free Atoms and Particles*; Academic: New York, 1980.
(3) Breckenridge, W. H. *Reactions of Small Transient Species*; Academic: New York, 1983; p 157.
(4) Breckenridge, W. H.; Umemoto, H. *Adv. Chem. Phys.* **1982**, *50*, 325.
(5) Hertel, I. V. *Adv. Chem. Phys.* **1980**, *42*, 325.
(6) Bottcher, C. *Adv. Chem. Phys.* **1980**, *42*, 169.
(7) Nikitin, E. E. *J. Chem. Phys.* **1965**, *43*, 744.
(8) Bjerre, A.; Nikitin, E. E. *Chem. Phys. Lett.* **1967**, *1*, 179.
(9) Bauer, E.; Fisher, E. R.; Gilmore, F. R. *J. Chem. Phys.* **1969**, *51*, 4173.
(10) Earl, B. L.; Herm, R. R. *J. Chem. Phys.* **1974**, *60*, 4568.
(11) Hershbach, D. R. *Adv. Chem. Phys.* **1966**, *10*, 319.
(12) Sevin, A.; Hiberty, P. C.; Lefour, J. M. *J. Am. Chem. Soc.* **1987**, *109*, 1845, and references cited therein.
(13) Chaquin, P. *J. Phys. Chem.* **1987**, *91*, 1440.
(14) Botschwina, P.; Meyer, W.; Hertel, I. V.; Reiland, W. *J. Chem. Phys.* **1981**, *75*, 5438.

0002-7863/88/1510-5681$01.50/0

Valence Bond Calculations. The theory we have used is usually refered to as multistructure valence bond. In this method, we first divide the supersystem into two fragments: Li and N_2. Then some fragment orbitals are determined by appropriate methods, which will be discussed below. The fragment orbitals (FOs) are AOs for the fragment Li and MOs for N_2. Then some valence bond structures (VBSs) are defined from these FOs, which are nonorthogonal when the fragments are close together, and the wave functions and energies of the ground and excited states are calculated by nonorthogonal CI among the so-defined VBSs. The wave function Ψ_i of a state I is now expressed as a linear combination of VBSs

$$\Psi_i = \sum_n C_{in}|V_n\rangle$$

and the weight W_{in} of each VBS V_n in the state I can be computed with the Chirgwin–Coulson formula[27]

$$W_{in} = C_{in}^2 + \sum_m C_{im}C_{in}\langle V_n|V_m\rangle$$

where the integral in broken brackets is the overlap between two VBSs, V_n and V_m.

Each VBS is associated to a chemical bonding scheme, i.e. a way to locate the electrons in orbitals and to couple them together. In what follows we define two categories of VBS: (i) the elementary ones, i.e. the VBSs that one usually writes by using the lower energy FOs, and (ii) the complementary ones, whose role is equivalent to optimize the FOs of each elementary VBS or in other words to compensate for the possible inadequacy of the orbitals used in the elementary VBSs. It is clear that complementary VBSs do not exist in minimal basis set and are unnecessary if elementary VBSs are built from perfectly adapted orbitals. Thus, the choices of orbitals and that of the VBSs are interrelated: The better the FOs, the smaller the number of VB structures.

1. Determination of the Fragment Orbitals. The orbitals of the Li fragment have been chosen so that each state of isolated lithium could be described by a single VBS. It is sufficient for that purpose to perform a CI on the lithium atom and to use the coefficient of the CI to transform the AOs as appropriate.

For N_2, different orbitals have been used for the Σ^+ and Π states.

(a) Σ^+ States. SCF orbitals would be perfect for N_2 in the asymptotic situation of infinite Li···N_2 distance, but they are expected to be less appropriate when both fragments come close to each other. Thus, it is necessary to complete the CI space with complementary VBSs, in which some occupied spin orbitals of the elementary VBSs are replaced by virtual ones, which should be of valence type, i.e. not too diffuse. One way to get rather contracted virtual orbitals is to use the GVB method,[28] which proved satisfactory in this respect. Another problem is that localized orbitals are needed for the lone pairs. Boys' procedure[29] can, of course, be used for occupied orbitals but not for the virtual ones. Once again, the GVB method is able to provide localized occupied and virtual orbitals, provided the virtual lone-pair orbitals are roughly prelocalized in the guess functions, to allow for the necessary symmetry breaking.

(b) Π States. So as to keep the asymptotic Π states similar to the Σ^+ ones, we kept the GVB occupied orbitals of N_2. Now the π^* virtual orbitals have to be diffuse so as to be able to receive an extra electron in the $Li^+N_2^-$ charge-transfer (CT) state; for this purpose the SCF virtual orbitals are perfect and have been used instead of the π_x^* and π_y^* GVB orbitals. The other virtual orbitals have been left unchanged. It should thus be noted that, in the CT state, the N_2^- fragment has the doubly occupied orbitals of N_2. Therefore, this inadequacy has to be compensated for by the addition of appropriate complementary VBSs.

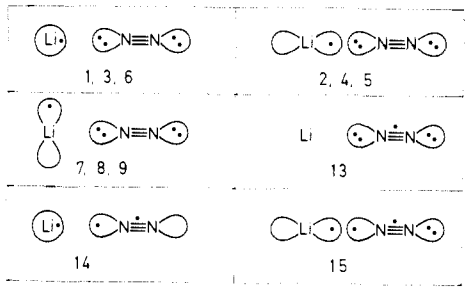

Figure 1. Some elementary valence bond structures. Structures **1–6** are of Σ^+ symmetry, while the other ones, **7–9** and **13–15**, are of Π symmetry.

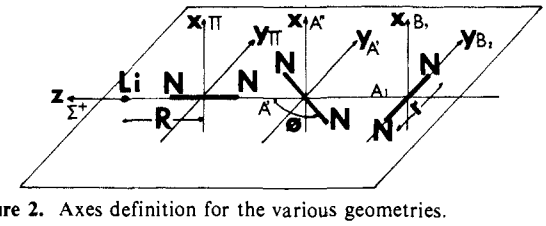

Figure 2. Axes definition for the various geometries.

2. Selection of VB Structures. In order to characterize each VBS, it is first useful to label the FOs. The 1s core orbitals will be omitted in all notations. The AOs of Li will be named ns, np_x, np_y, and np_z, n taking the values 2–4. The occupied MOs of N_2 will be labeled σ, π_x, π_y, n_l, and n_r, the latter two orbitals being localized lone-pair orbitals and n_l being nearest to the lithium atom. The antibonding orbitals will be labeled σ^*, π_x^*, and π_y^*, and since we use a split-valence basis set, each of the previously defined orbitals has an oscillatory counterpart. These latter virtual orbitals will be labeled σ', π_x', π_y', $\sigma^{*\prime}$, $\pi_x^{*\prime}$, $\pi_y^{*\prime}$, n_l', and n_r'.

(a) Σ^+ States. There are two kinds of elementary VBSs for Σ^+ states (see Figure 1), according to whether the lithium atom bears its single electron in an ns AO (structures **1**, **3**, and **6**) or in an np AO (structures **2**, **4**, and **5**). The numbering corresponds to the asymptotic order of stability of these VBSs (see Figure 10).

$\sigma^2\pi_x^2\pi_y^2n_r^2n_l^2 2s$ **1** $\quad$ $\sigma^2\pi_x^2\pi_y^2n_r^2n_l^2 2p_z$ **2** $\quad$ $\sigma^2\pi_x^2\pi_y^2n_r^2n_l^2 3s$ **3**

$\sigma^2\pi_x^2\pi_y^2n_r^2n_l^2 3p_z$ **4** $\quad$ $\sigma^2\pi_x^2\pi_y^2n_r^2n_l^2 4p_z$ **5** $\quad$ $\sigma^2\pi_x^2\pi_y^2n_r^2n_l^2 4s$ **6**

We have tested some complementary VBSs at the Li···N distance of 1.9 Å. Only the VBSs deduced from the elementary ones by the excitations ($\sigma \rightarrow s^*$), ($\pi_x \rightarrow \pi_x^*$), and ($\pi_y \rightarrow \pi_y^*$) proved to be efficient; this shows that the main effect of Li on the MOs of N_2 is to polarize them.

(b) Neutral Π States. The elementary VBSs (**7–12**) are those in which the lithium atom has its valence electron in an np_x or np_y orbitals. They

$\sigma^2\pi_x^2\pi_y^2n_r^2n_l^2 2p_x$ **7** $\quad$ $\sigma^2\pi_x^2\pi_y^2n_r^2n_l^2 3p_x$ **8** $\quad$ $\sigma^2\pi_x^2\pi_y^2n_r^2n_l^2 4px$ **9**

$\sigma^2\pi_x^2\pi_y^2n_r^2n_l^2 2p_y$ **10** $\quad$ $\sigma^2\pi_x^2\pi_y^2n_r^2n_l^2 3p_y$ **11** $\quad$ $\sigma^2\pi_x^2\pi_y^2n_r^2n_l^2 4p_y$ **12**

are of course degenerate two by two. The only efficient complementary VBSs are, for each structure **7–9**, those corresponding to a ($\pi_x \rightarrow np_x$) excitation, allowing some allyl-type resonance in the three-electron three-center π system, and the ($\pi_y \rightarrow \pi_y^*$) excitations (polarization of the remaining π bond). The other orbitals of N_2 are little affected by the presence of Li. Analogous complementary VBSs would of course be generated for structures **10–12**.

(c) Charge-Transfer State. A CT VBS (**13**) can be generated by removing the valence electron of the lithium atom and adding it to the π_x^* MO of N_2. Here a number of complementary VBSs are useful,

$\sigma^2\pi_x^2\pi_y^2n_r^2n_l^2\pi_x^*$ **13**

since N_2^- has the doubly occupied MOs of N_2. The excitations ($\pi_x \rightarrow$

(15) Sevin, A.; Chaquin, P. *Chem. Phys.* **1985**, *93*, 49.
(16) Chaquin, P.; Sevin, A.; Yu, H. T. *J. Phys. Chem.* **1985**, *89*, 2813.
(17) Bottcher, C. *Chem. Phys. Lett.* **1975**, *35*, 367.
(18) Amaee, B.; Bottcher, C. *J. Phys. B* **1978**, *11*, 1249.
(19) Kamke, W.; Kamke, B.; Hertel, I. V.; Gallagher, G. *J. Chem. Phys.* **1984**, *80*, 4879.
(20) Gislason, E. A.; Kleyn, A. W.; Los, J. *Chem. Phys.* **1981**, *59*, 91.
(21) Habitz, P. *Chem. Phys.* **1980**, *54*, 131.
(22) Staemmler, V. *Chem. Phys.* **1975**, *7*, 17.
(23) Peterson, M.; Poirier, R. *Monstergauss*; Department of Chemistry, University of Toronto: Toronto, Canada, 1981.
(24) Francl, M. M.; Pietro, W.; Hehre, W. J.; Binkley, J. S.; Gordon, M. S.; DeFrees, D. J.; Pople, J. A. *J. Chem. Phys.* **1982**, *77*, 3654. Gordon, M. S.; Binkley, J. S.; Pople, J. A.; Pietro, W. J. *J. Am. Chem. Soc.* **1982**, *104*, 2797. Pietro, W. J.; Francl, M. M.; Hehre, W. J.; DeFrees, D. J.; Pople, J. A.; Binkley, J. S. *J. Am. Chem. Soc.* **1982**, *104*, 5039.
(25) Huron, B.; Malrieu, J. P.; Rancurel, P. *J. Chem. Phys.* **1973**, *58*, 5745. Malrieu, J. P. *Theor. Chim. Acta* **1982**, *62*, 163. Evangelisti, S.; Daudey, J. P.; Malrieu, J. P. *Chem. Phys.* **1983**, *75*, 91.
(26) Davidson, E. R. *Chem. Phys. Lett.* **1973**, *21*, 565.
(27) Chirgwin, B. H.; Coulson, C. A. *Proc. R. Soc. London, A* **1950**, *201*, 196.
(28) Bobrowicz, F. W.; Goddard, W. A., III *Methods of Electronic Structure Theory*; Schaefer, H. F., III, Ed.; Plenum: New York, 1977; p 79.
(29) Boys, S. F. *Rev. Mod. Phys.* **1960**, *32*, 296.

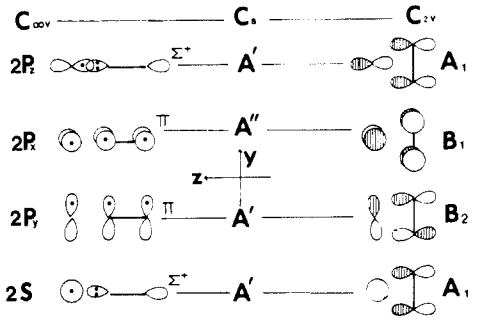

Figure 3. Schematic drawings of the leading VB structures that play a role in the process (left). On the right is drawn the phase relationship of the SOMOs, for various types of states. The symmetry correlations of Table I are recalled.

π_x'), ($\pi_y \rightarrow \pi_y'$), ($n_l \rightarrow n_l'$), and ($n_r \rightarrow n_r'$) are useful to optimize the degree of contraction of the MOs, and the excitations ($\pi_x \rightarrow \pi_x^*$) and ($\pi_y \rightarrow \pi_y^*$) polarize N_2 in the presence of Li^+. The ($\sigma \rightarrow \sigma^*$) excitation proved to be inefficient, showing that Li^+ only polarizes the π MOs. Two other elementary VBSs, **14** and **15**, have been included in the CI. They correspond to a back-donation of N_2^- to Li^+, by a transfer of an electron from a lone pair to a 2s or $2p_z$ orbital of Li.

$$\sigma^2\pi_x^2\pi_y^2n_r^2\pi_x^*n_l2s \qquad \sigma^2\pi_x^2\pi_y^2n_r^2\pi_x^*n_l2p_z$$
14 **15**

Of course, another degenerate CT exists, in which the singly occupied orbital of N_2^- is the π_y^*, as well as two elementary VBSs degenerate with **14** and **15**, deduced from the latter structures by exchanging the x and y subscript.

Topological Aspects of the Quenching Problem

Prior to a detailed analysis of the various electronic and energetic factors involved in the quenching mechanism, it is worth examining the topological features of the problem. First of all, in Figure 2 are displayed the various parameters and the labeling of MO and states of the triatomic systems. The (R, r, ϕ) set of geometrical parameters corresponds to the classical treatment of three-body systems. The point groups and the axis definitions for the three possible geometries have been selected so as to preserve the z axis throughout. This is improper for C_s geometry but has nevertheless been kept for the sake of simplicity. With those conventions, the axis symmetries within each point group are as indicated.

The schematic drawings of Figure 3 are of dual nature. Despite their very simple and intuitive meaning, they might be used as guidelines for further study in both MO–CI and VB formalisms. In some way, the system is described according to two limiting fashions: The diabatic one, on the left part, which freezes the electron localization into VB structures, and, on the right part, the classical MO-and-state picture, which upon CI yields the usual adiabatic potential energy surfaces. This dual aspect is emphasized on purpose, in the phase relationship that only appears in MO structures. Both kinds of formulation will be alternatively used for qualitatively depicting the leading features of a close approach, in various geometries.

(a) Linear Approach (Left Part). At short R, the GS of the system as well as the P_z excited component of Li* undergoes a repulsive three-electron interaction along the z axis. Some stabilization might possibly arise from back-donation in the π space. This way, N_2 donates electron density toward Li, and this kind of transfer results in a polarity that is contrary to the one expected to play a role in the quenching process. No tendency to observe some ($Li^+\cdots N_2^-$) character can be predicted for the GS in this geometry. The feature is different when dealing with the Π ($2P_x$, $2P_y$) components of Li*. The three electrons now lie on three 2P AOs, where allylic-type conjugation might play some stabilizing role. The overall stabilization is moreover accentuated, for, in those excited states, the preceding three-electron repulsion is replaced by a two-electron attraction. As an end result, the Π states are likely to yield exciplexes.

(b) C_{2v} Triangular Approach (Right Part). A schematic drawing of the SOMOs of the system in various states is displayed, in order to point out their dominant phase relationship. Due to symmetry constraint, both a_1 and b_1 MOs correspond to interaction of a Li AO with occupied π MOs of N_2, and, therefore, the corresponding SOMO more or less bears antibonding character. Only the b_2 SOMO, which results from a stabilizing interaction arising between $2P_y$ of Li and π_y^* of N_2, is bonding. A particular behavior is therefore expected for the corresponding $^2B_2$ state, which of course will deserve special attention in the coming discussion.

The situation is more complex in the C_s geometry. On the basis of MO-and-state terminology, we now have three states of A′ symmetry that will mix adiabatically upon bending. At short R the GS raising will push the other two upward, thus destabilizing the former B_2 or P_y states. The rearrangement of the π_x system along the $B_1 \Leftrightarrow A'' \Leftrightarrow P_y$ correlation bears strong analogy with the H_3 or Li_3 problems,[30] as long as only this π space is concerned. However, this behavior is very likely to be masked by the effects of the rest of the system, and it will not be further detailed.

A last point to be noted is that, either in C_{2v} or $C_{\infty v}$ geometries, crossings of the GS surface and the lowest excited ones, B_1, B_2, or Π, respectively, are allowed, while in the C_s geometry the GS can only adiabatically cross the A″ surface, all other crossings being avoided.

Reaction Coordinate as a Function of (R, r, ϕ)

A qualitative examination of the relative role of these parameters will be helpful in interpreting the complete set of calculated energy surfaces. It is convenient to consider three distinct regions, which can be characterized by the magnitude of R.

(a) $3 \leq R \leq \infty$ (Region 1). At large R, the overlap between the AOs of Li and those of N_2 is vanishing, and the calculations comfort the previous statement, which is common to most dynamical studies of quenching: the energy of the system, either in the GS or in the various excited states, is not ϕ dependent. When r is stretched, one observes a destabilization of N_2 that amounts to a translation at higher energy of all the low-energy states. The latter destabilization is larger than 0.5 eV when r is set equal to r_-, the equilibrium distance of N_2^- (see Table II). At infinite separation, the CT species Li^+/N_2^- is calculated at 8.03 eV (8.09 eV at the 6-31G* SCF level), for $r = r_0$. The $1/R$ electrostatic attraction energy raises from 0 to 4.80 eV in going from ∞ to 3 Å. It is therefore clear that when R lies in this range the latter attraction cannot overcome the endothermicity of the process leading from Li/N_2 to Li^+/N_2^-.

(b) $2.5 \leq R \leq 3$ (Region 2). In this region, the Li/N_2 overlap becomes noticeable and meanwhile the reaction coordinate (RC) becomes a complex function of R, r, ϕ. For the sake of simplicity and also in order to remain as close as possible to the early Nikitin's model, it is of practical use to consider two limiting situations. Setting ϕ at a constant value, for example 90 or 180°, we are left with two kinds of surfaces: those where $r = r_0$, which we call "covalent-type surfaces" for N_2 has its covalent equilibrium bond length, and those for which $r = r_-$, called "ionic-type surfaces" on the same premise. It should be noted that those surfaces actually are of complex nature and that the preceding appelation is only related to the value of r and does not presume of the polarity of the system, for any given state. Moreover, the ionic-type surfaces are likely to play a role in the excited states only, since a CT cannot result from the GS configuration (vide supra, the discussion of Figure 3).

For the lowest component of the excited state, both types of surfaces cross in region 2, as displayed in Figure 4. It is worth noting that this type of crossing is avoided in the C_s geometry, due to symmetry constraints, both surfaces having the same A′ symmetry (see Figure 3). The polarity of this type of species is reflected by the calculated atomic charges of the exciplexes shown in Figure 5. The data correspond to monoconfigurational SCF calculations, at the 3-21G level, and are only indicative. They nevertheless support the fact that when R becomes small, the

(30) In that case the distance from Li to the nearest N atom becomes very short.

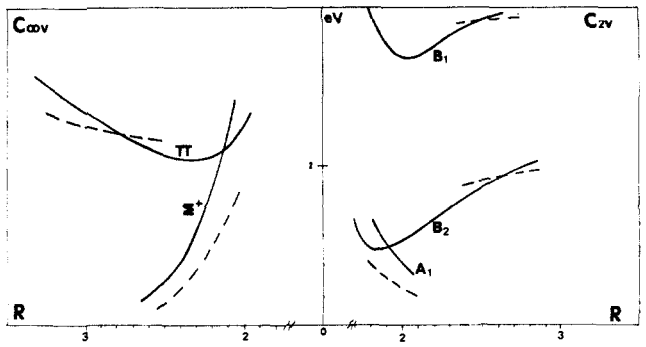

Figure 4. Detailed behavior of the lowest energy states in linear (left) and isoceles triangular geometries (right). In broken lines, the calculated potential energy curves correspond to nonrelaxed N_2, the full-line curves being obtained with an r distance of 1.169 Å, equal to the equilibrium bond length of N_2^-. The crossing between the Σ^+ and Π surfaces displayed in the left part corresponds to point Q, while the crossing between A_1 and B_2 surfaces in the right part corresponds to point P of Figure 8.

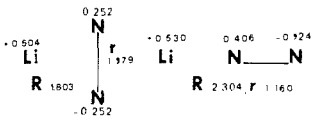

Figure 5. Optimized structures, at the 3-21G level, of the lowest energy exciplexes in C_{2v} and $C_{\infty v}$ geometries. The atomic charges are those of the SCF step without CI.

optimal RC becomes r dependent and is best described when $r = r_-$. The aforementioned crossings occur at 2.8 Å in the $C_{\infty v}$ geometry and at 2.45 and 2.65 Å, respectively, for the B_1 and B_2 states in the C_{2v} geometry. The features exhibited by those surfaces will be discussed in detail later on.

(c) $R \leq 2.5$ (Region 3). In this region, one observes that the ionic-type surfaces are systematically at lower energy than their covalent counterparts, in the excited states, the reverse being true in the GS. This situation largely favors their possible contact and, for this reason, in region 3, the RC is only a function of R and ϕ, r being set equal to r_-.

SCF-CI Energy Surfaces

After the preceding discussion, at given ϕ, the sets of ESs can be divided into three typical parts. This partition of the RC is of practical use and will be followed in all the forthcoming discussions. Some general trends, common to all types of geometries, can be first pointed out. In region 1, a weakly attractive complex is observed for the GS, in the $C_{\infty v}$ geometry. When ϕ changes toward the C_{2v} geometry, no such complex is observed. In the GS, the facility of approach varies according to the sequence $C_{\infty v} < C_s < C_{2v}$. In the excited state, a strong stabilization is observed for the lowest Π and B_2 states in $C_{\infty v}$ and C_{2v} geometries respectively. This trend is less pronounced for the higher energy states of the same symmetry. In the meantime, the lowest Σ^+, A′, or A_1 excited states are destabilized. The most striking feature is observed at high energy ($\geq$5 eV), where the CT states steeply descend when R decreases, and doing so, intend to cross valence states, thus increasing the downward behavior of the low-lying excited states of same symmetry. This is clearly shown in Figures 6 and 7 where the calculated ESs for $C_{\infty v}$ and C_{2v} geometries are reported.

(a) Linear RC ($C_{\infty v}$). In region 2, the behavior of the lowest lying states, already displayed in Figure 4, has been progressively leveled and thus does not exhibit a broken aspect as expected for adiabatic ESs. The GS and the first excited Σ^+ states are mostly repulsive when R decreases. This is no longer the case for the higher energy 3S and 3P states of same symmetry, for which a weak attraction is observed in regions 1 and 2, with respect to infinite separation. The latter behavior can be qualitatively explained on the following grounds: the overall three-electron repulsion, which dominates in the valence states (see Figure 3, 2S and $2P_z$ components), is largely balanced in the Rydberg states (3S, $3P_z$) by electrostatic attraction. Indeed, the latter states

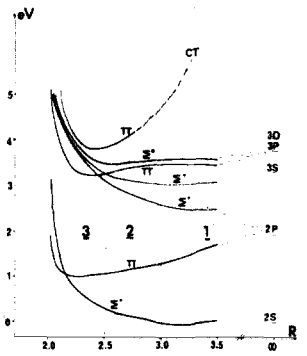

Figure 6. MO-CI calculated potential energy surfaces in the linear geometry. In region 1 the reaction coordinate is only a function of R, r being set equal to r_0. In region 3, the reaction coordinate is also a function of R, r being set equal to r_-. In region 2, we have linearly varied r from r_0 to r_-. This procedure thus allows for a smooth variation of the surface profiles.

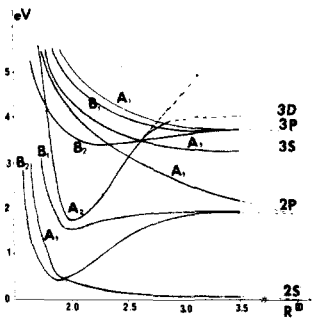

Figure 7. MO-CI calculated potential energy surfaces in isoceles triangular geometry. The same smooth r variation as described in Figure 6 has been used, between 3.0 and 2.5 Å.

roughly correspond to an electron orbiting far from a positive Li^+ core, thus allowing for a rather attractive approach at medium value of R. On the other hand, the Π states, either valence or Rydberg in character, are attractive, up to a very small (Li···N) distance.[30] The CT state reaches the Li* (3D) energy range at the frontier of regions 1 and 2. Several avoided crossings occur which prevent this state from descending too much in energy. In turn, those intended crossings have strong consequences for the lowest states, which reflect this tendency upon CI, the main effect being the admission of some ionic character in valence states.

(b) Isoceles Triangular RC (C_{2v}). Some differences with the $C_{\infty v}$ ESs are worthy of comment. Keeping in mind the correlations of Table I, we see that all the A_1 states are repulsive upon decrease of R. The splitting of the Π states degeneracy yields B_1 and B_2 states, the valence components of which give rise to exciplexes. As anticipated by the nature of the SOMOs displayed in Figure 3, the B_2 state is much more stabilized than its B_1 partner. This behavior is reflected in the higher states where no stabilization is found for the lowest B_1 Rydberg state, while an exciplex exists on the parent B_2 ES. The CT states widely differ from those of the $C_{\infty v}$ geometry: The B_2 component is absent in the drawing due to efficient avoided crossings with high-energy states, while the A_2 component steeply descends without crossing Rydberg states since none has such symmetry. The unique crossing occurs with the component of the 3D state of Li*, and, therefore, the corresponding ES quite exhibits the behavior of an unperturbed CT.

Qualitative Mechanism of the Quenching

Dealing with the quenching mechanism the behavior of the GS and the lowest energy excited state is essential. When we go back to Figure 4, it is worth comparing the $C_{\infty v}$ and C_{2v} processes in a quantitative way. First of all, the Π and B_2 surfaces reveal similar trends, each having a contact point with the GS, along their ionic-type surfaces, at energies that are far below that of the initial 2P state of Li. This is no longer the case for the B_1 component in C_{2v} geometry, which only yields a weakly stabilized exciplex at 1.66 eV. The B_2 exciplex is much more stable than

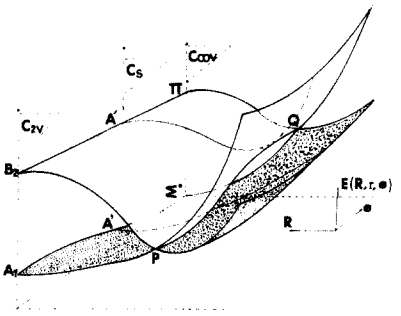

Figure 8. Perspective view showing the behavior of one component of the lowest Π MO–CI potential energy surfaces. It corresponds to the Π ⇔ A′ ⇔ B_2 correlation. Two points of contact exist, in P and Q, with the GS surface. In between, both surfaces, having the same A′ symmetry, avoid themselves. The profile of the surfaces is derived from Figure 6.

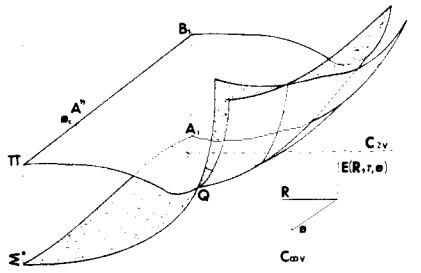

Figure 9. Same legend as Figure 8, for the Π ⇔ A″ ⇔ B_1 correlation of the same Π excited state. Here, instead of two points, we have a contact region with the GS surface, starting from point Q (linear geometry), to the point corresponding to the bent structure with $\phi = \phi_c$. Beyond this critical point, both surfaces avoid themselves.

the Π one: 0.46 and 1.03 eV, respectively, with respect to the GS zero energy. The formation of an isoceles triangular exciplex is therefore largely preferred. If one recalls the previous discussion of the correlations of Figure 3, it is conspicuous that the C_s geometry differs from the preceding two ones: no adiabatic contact is possible between the GS and the lowest energy excited states, both of A′ symmetry. When this is kept in mind, it is now possible to topologically depict the complete behavior of the system in regions 2 and 3, for the couple of states of lowest energy. This purpose is achieved in Figures 8 and 9 where three-dimensional overviews are displayed in a pictorial fashion so as to emphasize the salient strokes.

(a) Π ⇔ A′ ⇔ B_2 Surface (Figure 8). The two parallel horizontal axes correspond to C_{2v} and $C_{\infty v}$ geometries, and the diagonal axis is related to ϕ variation from 90 to 180°. The A_1/B_2 and Σ^+/Π contacts taking place in both geometries are labeled P and Q, respectively. Between P and Q, the corresponding crossing is avoided, yielding a bridge pattern as displayed. Point P is at lower energy than Q, and thus, its neighborhood constitutes an attractor for the excited surface, which, in some way, is drained toward this region rather than toward Q. Once the system has reached point P, a switch to the A_1 surface is possible through internal conversion. The corresponding vibrational coupling matrix element has the form $\langle A_1|\delta/\delta Q|B_2\rangle$,[31] where $\delta/\delta Q$ has the symmetry of the vibration. For this element not to vanish by symmetry, it is required that the vibration have the B_2 symmetry, that is, a nonsymmetrical distortion of the system.[32] This motion drives the system to the GS surface, and since the triangular approach is the less favorable one, it will gain further rotational energy when the fragments separate, along with some recoil energy. At point Q, the electronic motion, which couples the Σ^+ and Π surfaces, is of π symmetry, i.e. likely to induce bending of the system, and thus, mostly vibrational energy will result from this internal conversion.

(b) Π ⇔ A″ ⇔ B_1 Surface (Figure 9). The pattern is simpler than in the B_2 case since, for energy reasons, only a small contact region is located around point Q, the limit of which corresponds to ϕ_c (≃150–160°). Starting from the upper surface, the system is driven toward point Q where it can reach the GS surface. Around the C_{2v} exciplex, it should be noted that the internal conversion matrix element is near zero since, in $\langle A_1|\delta/\delta Q|B_1\rangle$, the vibration cannot have the B_1 symmetry, which does not exist in a triatomic arrangement. As an end result, the dominant process is likely to mostly consist in red-shifted fluorescence of Li*.

We thus have a quantitative model for quenching at low energy, based on the analysis of adiabatic surfaces. Although we have seen that the so-called ionic-type surfaces play an essential role in surface contact, we still do not know exactly what is the actual ratio of the covalent to ionic mechanism. In reality, both aspects are drowned in the full-electron correlation calculation, due to the huge number of terms appearing in the Møller–Plesset perturbation. The coming chapter will bring a clear and simple answer to this important question. We are left with the problem of the A_2 exciplex displayed in Figure 7. First of all, this state can be populated from low-lying states through the two following ways:

$$A_2 \text{ electronic} \times B_2 \text{ vibration} \times A_2 \text{ electronic} \in A_1$$

$$A_2 \text{ electronic} \times A_1 \text{ vibration} \times A_2 \text{ electronic} \in A_1$$

The latter one involves a 3D excitation of Li while the former can be done via the $3P_x$ Rydberg component. Were this state populated, it would not couple with the GS, since no A_2 vibration is available: Fluorescence would be the dominant deactivation process.

Valence Bond Calculations and Results

The ensemble constituted of one elementary VBS and its complementary structures defines a subspace in which a nonorthogonal CI can be performed. The lowest root of this limited CI constitutes what we will call a quasi-diabatic state, to avoid confusion with the denomination "diabatic", which usually refers to states ϑ, ϑ' satisfying the condition $\langle\vartheta|\delta/\delta Q|\vartheta'\rangle = 0$, which is not the case here. So defined, a quasi-diabatic state is a variationally optimized wave function corresponding to a chemical bonding scheme. In the asymptotic limit of infinite Li···N_2 distance, the quasi-diabatic states merge with the adiabatic ones, and the latter correspond to avoided crossings of the former at short distances. In the coming section, we have restricted ourselves to linear geometries without relaxation of N_2 bond length. Thus, the VB calculations presented here have to be considered as a model, aimed at illustrating the respective roles of neutral and ionic configurations in the quenching process. This restriction was justified by the fact that SCF electron population analyses displayed in Figure 5 show that the net charge separation in linear and triangular exciplexes are comparable, thus leading to infer that the ionic and covalent structures play similar roles in both geometries.

(a) Σ^+ States. We will label 2S, $2P_z$, 3S, $3P_z$, $4P_z$, and 4S, respectively, the quasi-diabatic states described by the elementary VBSs **1**–**6**. Each quasi-diabatic state is comprised of one elementary VBS and three complementary ones (vide supra). Their energy is plotted agains the Li···N_2 distance in Figure 10.

Interestingly, it appears that the two lowest quasi-diabatic states do not behave as the higher ones. Indeed, as Li approaches N_2, the 2S and $2P_z$ states are destabilized, a consequence of the repulsion between the singly occupied 2s or $2p_z$ AO of Li and the lone pair of N_2. But this effect holds no longer when the singly occupied orbital of Li is diffuse, as now the system looks like an Li···N_2 entity with a remote extra electron. Li^+ is slightly attracted by the N_2 lone pair, and the consequence is that the four 3S, $3P_z$, $4P_z$, and 4S quasi-diabatic states display a shallow potential well. The 3S state even crosses the $2P_z$ one at short distance. This

(31) Applications of these concepts to chemical reactions is found in: Lee, T. S. *J. Am. Chem. Soc.* **1977**, *99*, 3909, and basic references cited therein.

(32) Herzberg, G. *Infrared and Raman Spectra of Polyatomic Molecules*; Van Nostrand: Princeton, NJ, 1966; pp 106 and 107. The *XZ* plane is used as the molecular plane, so that his B_1 species corresponds to our B_2 species.

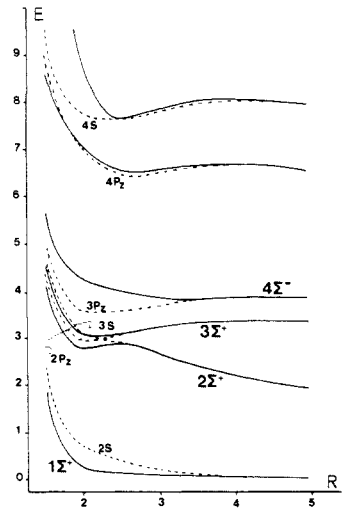

Figure 10. Potential energy surfaces of the states of Σ^+ symmetry, calculated by the valence bond method. The reference energy corresponds to −116.297 85 au. The geometry is linear, with the N_2 bond length fixed at its equilibrium value: dotted lines, quasi-adiabatic states before avoided crossing; full lines, adiabatic states.

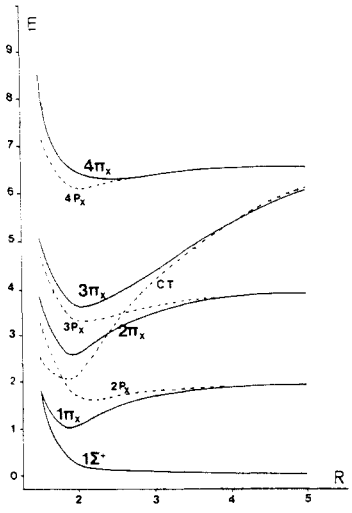

Figure 11. Energy surfaces of the excited states of Π symmetry, along with the Σ^+ ground state. Same geometry and reference energy as in Figure 10: dotted lines, quasi-diabatic states before avoided crossing; full lines, adiabatic states.

crossing is of course avoided by the $2\Sigma^+$ and $3\Sigma^+$ adiabatic states, and, as a consequence, they are separated by a very small gap, the former displaying a bump and the latter an exciplex.

On the other hand, the $1\Sigma^+$ adiabatic state is, of course, less repulsive than the 2S quasi-diabatic state, because it is stabilized by some $2P_z$ component. In other words, the $1\Sigma^+$ state can be described as an N_2 molecule interacting with a Li atom bearing an electron in an hybrid orbital, which bears more and more p character as the interacting distance is shorter, and is oriented in the direction opposite to N_2, so as to minimize the electronic repulsion.

(b) Π States. The potential energy curves of the adiabatic and quasi-diabatic Π_x states are reported in Figure 11, together with the $1\Sigma^+$ ground-state energy curve. The neutral quasi-diabatic states are labeled $2P_x$, $3P_x$, and $4P_x$ while the charge-transfer one is refered to as CT. All the Π states are, of course, doubly degenerate.

It appears that the $2P_x$, $3P_x$, and $4P_x$ neutral states display an exciplex, due to a stabilizing interaction, of allyl-type, between the singly occupied AO of Li and the π_x MO of N_2. However, the $2P_x$ state remains far from the ground state and cannot induce, by itself, the quenching phenomenon.

On the other hand, the behavior of the CT is illuminating. As Li approaches N_2, it goes down and crosses the $2P_x$ and $3P_x$ states before the very repulsive region, in agreement with Nikitin's mechanism. As a result of an avoided crossing, the $1\Pi_x$ state displays a deep exciplex and comes very close to the ground-state surface, thus explaining the quenching. The role of the CT state would be even more emphasized, in Figure 11, if N_2 were allowed to be stretched to the N_2^- geometry. As we kept the N···N distance of neutral N_2 throughout the VB calculations, the importance of the CT state in the quenching phenomenon, as exemplified in our VB diagram, can be considered as a lower limit. Relaxing the N···N distance in the $1\Pi_x$ state at short distance, one would get the $(1\Pi_x-1\Sigma^+)$ crossing, which is observed in the MO–CI calculations (vide supra).

The $1\Pi_x$ adiabatic state naturally gains some ionic character as Li approaches N_2, to reach an ionic:covalent ratio of 44:56 at the bottom of the potential well. The $2\Pi_x$ state, first purely covalent in the asymptotic limit, becomes purely ionic at a Li···N_2 distance of 2.5 Å and goes down, up to the vicinity of the $2P_x$ CT crossing, where its ionic:covalent ratio amounts to 33:67. The $3\Pi_x$ adiabatic state, first purely ionic at large Li···N_2 distances, becomes mainly covalent, with an ionic:covalent ratio of 16:84, near the bottom of its potential well.

Conclusion

The qualitative predictions regarding the formation of exciplexes deduced from simple considerations of either VB structures or MOs displayed in Figure 3 are confirmed by calculations. The MO–CI surfaces show important different features in the C_{2v} and $C_{\infty v}$ geometries. The most efficient quenching arises in the B_2 component of the triangular geometry. However, a contact point with the GS is also observed at higher energy in the linear arrangement. The stretching of N_2 provides an efficient way for linking the GS and the lowest excited state in both cases. The role of the charge transfer is emphasized, but its relative importance with respect to covalent structures cannot be extracted from MO–CI calculations. Those findings are first of all nicely confirmed by VB calculations, which, moreover, yield a clear knowledge of the respective roles of the ionic and covalent structures in the overall quenching process. The model VB study shows that, for the lowest excited-state exciplex, the charge-transfer amounts to nearly 50%. Both types of approaches predict that this sizable ionic character will induce important vibrational and rotational relaxations as an end result of the whole process.

Acknowledgment. We are indebted to J. M. Lefour and J. P. Flament who have written the valence bond program and made it available to us.

Registry No. Li^+, 17341-24-1; Li, 7439-93-2; N_2, 7727-37-9.